



Article

Ultra-Low Thermal Conductivity and Improved Thermoelectric Performance in Tungsten-Doped GeTe

Zhengtang Cai ^{1,2} , Kaipeng Zheng ^{1,2}, Chun Ma ^{1,2}, Yu Fang ^{1,2}, Yuyang Ma ¹, Qinglin Deng ^{1,2,*} and Han Li ^{1,2,*}

¹ School of Physics and Materials Science, Guangzhou University, Guangzhou 510006, China; zt.caine@e.gzhu.edu.cn (Z.C.); 2112119106@e.gzhu.edu.cn (K.Z.); 2112119081@e.gzhu.edu.cn (C.M.); 2112219110@e.gzhu.edu.cn (Y.F.); 32119600037@e.gzhu.edu.cn (Y.M.)

² Research Center for Advanced Information Materials (CAIM), Huangpu Research & Graduate School of Guangzhou University, Guangzhou 510555, China

* Correspondence: qldeng@gzhu.edu.cn (Q.D.); lihan@gzhu.edu.cn (H.L.)

Abstract: Compared to SnTe and PbTe base materials, the GeTe matrix exhibits a relatively high Seebeck coefficient and power factor but has garnered significant attention due to its poor thermal transport performance and environmental characteristics. As a typical p-type IV–VI group thermoelectric material, W-doped GeTe material can bring additional enhancement to thermoelectric performance. In this study, the introduction of W, Ge_{1-x}W_xTe ($x = 0, 0.002, 0.005, 0.007, 0.01, 0.03$) resulted in the presence of high-valence state atoms, providing additional charge carriers, thereby elevating the material's power factor to a maximum PF_{peak} of approximately $43 \mu\text{W cm}^{-1} \text{K}^{-2}$, while slightly optimizing the Seebeck coefficient of the solid solution. Moreover, W doping can induce defects and promote slight rhombohedral distortion in the crystal structure of GeTe, further reducing the lattice thermal conductivity κ_{lat} to as low as approximately $0.14 \text{ W m}^{-1} \text{K}^{-1}$ ($x = 0.002$ at 673 K), optimizing it to approximately 85% compared to the GeTe matrix. This led to the formation of a p-type multicomponent composite thermoelectric material with ultra-low thermal conductivity. Ultimately, W doping achieves the comprehensive enhancement of the thermoelectric performance of GeTe base materials, with the peak ZT value of sample Ge_{0.995}W_{0.005}Te reaching approximately 0.99 at 673 K, and the average ZT optimized to 0.76 in the high-temperature range of 573–723 K, representing an increase of approximately 17% compared to pristine GeTe within the same temperature range.

Keywords: GeTe; ultra-low thermal conductivity; synergistic effects; multiscale materials; electronic engineering



Citation: Cai, Z.; Zheng, K.; Ma, C.; Fang, Y.; Ma, Y.; Deng, Q.; Li, H. Ultra-Low Thermal Conductivity and Improved Thermoelectric Performance in Tungsten-Doped GeTe. *Nanomaterials* **2024**, *14*, 722. <https://doi.org/10.3390/nano14080722>

Academic Editor: Maria Grazia Musolino

Received: 31 March 2024

Revised: 18 April 2024

Accepted: 18 April 2024

Published: 20 April 2024



Copyright: © 2024 by the authors. Licensee MDPI, Basel, Switzerland. This article is an open access article distributed under the terms and conditions of the Creative Commons Attribution (CC BY) license (<https://creativecommons.org/licenses/by/4.0/>).

1. Introduction

Thermoelectric (TE) materials have attracted considerable attention as environmentally friendly and green energy materials due to their ability to directly convert thermal energy into electrical energy. The performance of TE materials is typically assessed using the dimensionless figure of merit ZT, defined as $ZT = S^2 \sigma T / \kappa_{\text{tot}}$, where S represents the Seebeck coefficient, σ is the electrical conductivity, T is the temperature in Kelvin, and κ_{tot} denotes the total thermal conductivity (the sum of the lattice thermal conductivity and electronic thermal conductivity, i.e., $\kappa_{\text{tot}} = \kappa_{\text{lat}} + \kappa_e$). The optimization of TE material performance primarily involves tuning the carrier concentration to enhance the electrical transport properties and improving the phonon transport characteristics to reduce the lattice thermal conductivity [1–3], thereby increasing the power factor and ultimately enhancing the thermoelectric performance of the material [4,5].

In recent years, GeTe has emerged as a typical IV–VI group semiconductor thermoelectric material [6]. Benefiting from its crystal structure closely resembling that of SnTe [7–9] and PbTe [10–12], GeTe exhibits a relatively high intrinsic Seebeck coefficient. However, due to the environmental toxicity of PbTe, poor mechanical and thermoelectric properties of SnTe, and the fact that the peak ZT value of GeTe-based materials can exceed 0.8 in

the temperature range of 300–750 K, GeTe has become a hot topic in thermoelectric research. Nevertheless, the intrinsic electrical properties of GeTe are generally suboptimal, its thermal stability is inadequate, and its thermal transport performance is poor, limiting its widespread application. GeTe possesses a narrow bandgap structure and exhibits different crystal structures at different temperatures: it adopts a rhombohedral crystal structure (r-GeTe) at room temperature and a cubic crystal structure (c-GeTe) at high temperatures, with a phase transition from r- to c-GeTe occurring around ~ 700 K [3,13]. We also realized that a slight rhombohedral distortion occurs along the [1 1 1] crystal axis direction [14], which results in the convergence of the valence band [8,12,15]. Nevertheless, the phase transition is detrimental to the thermoelectric properties of GeTe materials as it likely results in the additional loss of electron energy due to extensive lattice deformation. This, in turn, negatively impacts carrier mobility, affecting the figure of merit (ZT). Essentially, the primary goal of thermoelectric material optimization is to increase the ZT value, which can be achieved by reasonably regulating the coupling relationship between the three thermoelectric performance parameters: S , σ , and κ_{tot} . When the electrical conductivity of the sample is increased, its electronic thermal conductivity also increases. However, excessively high electrical conductivity has a detrimental impact on carrier mobility, resulting in a decreasing Seebeck coefficient and affecting the thermoelectric properties of the material. Therefore, the key to improving the ZT value of materials lies in synergistically regulating the electrical and thermal transport properties. In order to optimize the thermoelectric properties of GeTe-based materials, researchers typically employ doping or alloying techniques. In doping engineering, the carrier concentration and energy band structure of the material can be optimized by applying donor doping, which results in a larger Seebeck coefficient and a higher power factor. Furthermore, doping engineering can result in the introduction of point defects, dislocations, and grain boundary defects, which lead to lattice distortions in GeTe material. This intensifies phonon scattering within the material and reduces the lattice's thermal conductivity, thereby further increasing the ZT value.

In our previous work, it was demonstrated that tungsten (W) doping can effectively enhance the electrical conductivity of the material, resulting in the optimization of a higher power factor and the capacity to elevate the Seebeck coefficient [16]. Regarding thermal transport properties, previous research has demonstrated that W doping can also introduce a multitude of grain boundary and dislocation defects, a considerable number of which can enhance phonon scattering in the material, resulting in a significant reduction in the lattice thermal conductivity and, ultimately, a dramatic optimization of the ZT value.

Consequently, the present study aims to achieve the same optimization via the elemental tungsten (W) doping of a GeTe system [17]. It is noteworthy that the electrical and thermal transport properties of GeTe-based materials can be modulated by designing W substitution (donor doping). Firstly, the intervention of W substitution introduced high-valence atoms, resulting in an increase in the power factor of the samples across the entire temperature range due to the introduction of additional carriers. Secondly, W also exists in the solid solution of $\text{Ge}_{1-x}\text{W}_x\text{Te}$ ($x = 0, 0.002, 0.005, 0.007, 0.01, 0.03$) in the form of W atoms [18–20], forming defects to replace some of the Ge vacancies [21–23]. On the other hand, the formation of defects further strengthens the scattering of phonons in the material [24–26], significantly reducing the lattice thermal conductivity. Ultimately, we achieved a significant improvement in the peak power factor (PF_{peak}) at 673 K up to $\sim 43 \mu\text{W cm}^{-1} \text{K}^{-2}$ and the optimization of the ultra-low lattice thermal conductivity of $0.14 \text{ W m}^{-1} \text{K}^{-1}$ at 673 K for a W doping concentration of $x = 0.002$. This contributes to a remarkable enhancement in the average ZT value up to ~ 0.76 within the temperature range of 573–723 K and represents a 17% increase compared to the GeTe matrix, thereby improving the thermoelectric performance of GeTe-based materials overall [7,9,27].

2. Materials and Methods

2.1. Materials and Synthesis

This study involved the preparation of $\text{Ge}_{1-x}\text{W}_x\text{Te}$ ($x = 0, 0.002, 0.005, 0.007, 0.01, 0.03$) compounds in an inert gas (Ar) atmosphere within a glovebox. High-purity elements Ge (99.999%, Aladdin, Shanghai, China), W (99.99%, Aladdin), and Te (99.99%, Aladdin) were accurately weighed and transferred into graphite crucibles, thoroughly mixed, and then packed into quartz glass tubes. Subsequently, the tubes were sealed under high vacuum conditions (below 10^{-5} Torr). The loaded quartz tubes were then placed in a box furnace and slowly heated to 1373 K, maintained for 12 h, followed by quenching with water to room temperature. Subsequently, the temperature was raised again to 923 K for annealing over 3 days, and finally slowly cooled to room temperature. The resulting alloy ingots were carefully removed and manually ground into fine powders using an agate mortar and pestle. Appropriate amounts of the ground powders were weighed and loaded into prepared graphite molds, which were then placed into a spark plasma sintering furnace (SPS, KCE-FCT HPD10, Sachsenheim, Germany) for vacuum hot-pressing sintering. During the sintering process, the samples were subjected to a uniaxial pressure of 60 MPa in a high vacuum, heated to 573 K in 5 min, and then heated to 823 K in 3 min. Finally, they were held for 5 min before being removed and allowed to cool naturally.

2.2. Measurement and Characterizations

After SPS sintering and subsequent cooling, the samples were subjected to wire cutting to produce rectangular prismatic specimens measuring $12 \times 3 \times 3$ mm. These specimens were then lightly polished and placed into a four-probe thermoelectric measurement system (CTA, CRYOALL CTA-3S, Beijing, China) to simultaneously measure the temperature-dependent electrical conductivity σ and Seebeck coefficient S . Additionally, the thin discs obtained from SPS sintering underwent thermal diffusivity testing using the Laser-Flash Thermal Conductivity Instrument (LFA 467 HT NETZSCH, Tannesstein, Germany) to determine the thermal diffusivity coefficient D of the samples. Subsequently, the density ρ of each sample was determined using the Archimedes' displacement method. The total thermal conductivity κ_{tot} of the samples was calculated using the formula $\kappa_{tot} = D\rho C_p$, where C_p represents the theoretical specific heat capacity of the GeTe material. Furthermore, the electronic thermal conductivity κ_e of the samples was calculated according to the Wiedemann–Franz law and the formula $\kappa_e = L\sigma T$. Finally, the lattice thermal conductivity κ_{lat} of the samples was obtained by subtracting κ_e from κ_{tot} . Subsequently, X-ray diffraction (XRD) analysis was conducted at room temperature using a Rigaku Smartlab 9 KW (Tokyo, Japan) instrument to perform the compositional analysis of the samples. To further understand the influence of the microstructural composition of the samples on the thermoelectric properties of the GeTe materials, a transmission electron microscopy (TEM, FEI HELIOS 5CX, Hillsboro, OR, USA) characterization test was performed to observe and analyze the mechanism.

3. Results and Discussion

The room temperature powder X-ray diffraction (XRD) results of the $\text{Ge}_{1-x}\text{W}_x\text{Te}$ samples ($x = 0, 0.002, 0.005, 0.007, 0.01, 0.03$) are depicted in Figure 1a. It can be observed that upon W doping into GeTe, most of the diffraction peaks match well with the rhombohedral phase single-phase structure of r-GeTe (space group: $R3m$, PDF: 47-1079). In Figure 2a,b, the slight precipitation of Ge can be observed at low angles of $25\sim 26^\circ$ and $42\sim 44^\circ$, respectively. This phenomenon is commonly observed throughout the entire GeTe system and is attributed to the presence of large Ge vacancies in the GeTe system, consistent with previous reports [3,28,29], which do not significantly affect the ultimate thermoelectric performance of GeTe-based materials [2,24,30]. The appearance of dual peaks of GeTe at this angle further confirms its rhombohedral structure at room temperature. Moreover, the sample $\text{Ge}_{0.97}\text{W}_{0.03}\text{Te}$ exhibits a distinct second-phase diffraction peak at $\sim 40^\circ$ in Figure 1b. Through XRD spectrum analysis and data comparison, the main component

of the diffraction peak at this angle is identified as W (space group: $Im\bar{3}m$, PDF: 04-0806), indicating a solubility of W in the GeTe system of approximately 0.5 mol%. Additionally, GeTe undergoes a phase transition from the r- to the c-GeTe (c-GeTe, space group: $Fm\bar{3}m$) at ~ 700 K, transforming its crystal structure along the $[1\ 1\ 1]$ direction into a cubic structure, which is similar to that of PbTe [31] and SnTe [1,20]. This cubic structure is also similar to the crystal structure of the precipitated W phase in this study, suggesting structural similarity with GeTe [32].

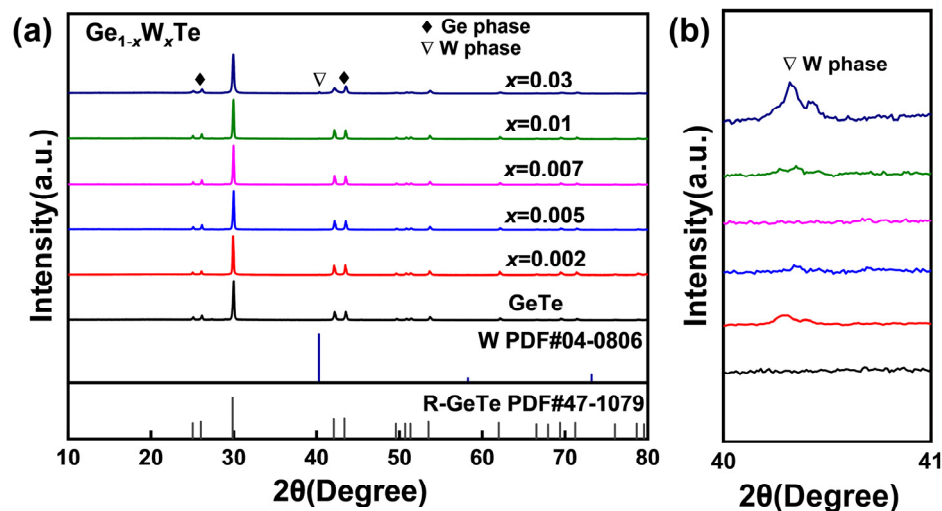


Figure 1. (a) Room temperature powder XRD patterns of the $Ge_{1-x}W_xTe$ ($x = 0, 0.002, 0.005, 0.007, 0.01, 0.03$) samples; (b) enlarged view of the W phase at $40\sim 41^\circ$.

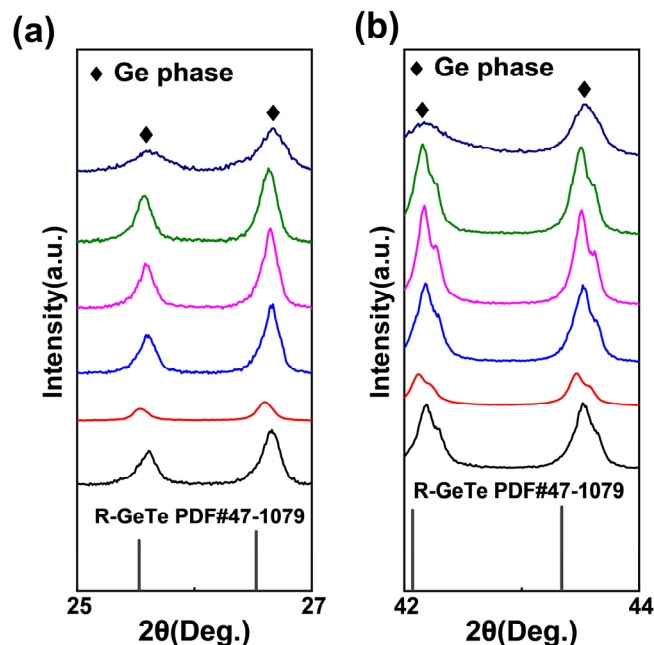


Figure 2. Room temperature powder XRD patterns enlarged view of the Ge phase of the $Ge_{1-x}W_xTe$ ($x = 0, 0.002, 0.005, 0.007, 0.01, 0.03$) samples (a) at $25\sim 27^\circ$; (b) enlarged view at $42\sim 44^\circ$.

Upon W doping in GeTe, the electrical transport properties of the material undergo subtle changes. In Figure 3a, as the proportion of W doping increases, the electrical conductivity (σ) exhibits a trend of initially decreasing and then increasing. Compared to the GeTe matrix, when $x = 0.002$, the σ of the sample $Ge_{0.998}W_{0.002}Te$ decreases to $\sim 1.8 \times 10^3$ S cm^{-1} at 723 K. When $x > 0.005$, the σ of the sample $Ge_{1-x}W_xTe$ increases with the amount of W doping, and at $x = 0.03$, the σ of the sample $Ge_{0.97}W_{0.03}Te$ is higher than

that of other samples and higher than the GeTe matrix overall. This may be attributed to the introduction of the high-valence state W into GeTe, providing additional charge carriers and resulting in an increase in the carrier concentration. In Figure 3c, a schematic diagram of the Seebeck coefficient (S) of the sample $\text{Ge}_{1-x}\text{W}_x\text{Te}$ ($x = 0, 0.002, 0.005, 0.007, 0.01, 0.03$) as a function of temperature is presented. In the mid-low temperature range (300–573 K), the S of the sample $\text{Ge}_{0.995}\text{W}_{0.005}\text{Te}$ shows a certain improvement, reaching $\sim 154 \mu\text{V K}^{-1}$ at 723 K. When $x \geq 0.005$, S begins to decline, especially when $x = 0.03$, the sample $\text{Ge}_{0.97}\text{W}_{0.03}\text{Te}$ exhibits a significant reduction in S in the high-temperature range (600–750 K). This may be because W has reached its solubility limit in the GeTe system, existing in the material structure in the form of W. Additionally, as W belongs to heavy atoms, it affects carrier mobility. In Figure 3d, the power factor PF of the sample $\text{Ge}_{0.998}\text{W}_{0.002}\text{Te}$ is lower than that of the undoped sample GeTe, and when the doping level rises to $x = 0.005$, the PF of the sample $\text{Ge}_{0.995}\text{W}_{0.005}\text{Te}$ is higher than that of the undoped GeTe matrix, with a peak value reaching $\sim 43 \mu\text{W cm}^{-1} \text{K}^{-2}$. When the W doping ratio is greater than $x = 0.005$, the PF of the sample $\text{Ge}_{1-x}\text{W}_x\text{Te}$ decreases with the increase in the doping concentration. This phenomenon occurs because W doping introduces additional heavy atoms into the GeTe material, significantly affecting the electrical transport properties of the sample [5,33,34]. Despite the weak increase in the Seebeck coefficient of the sample $\text{Ge}_{0.995}\text{W}_{0.005}\text{Te}$, W doping leads to a higher peak PF in the material compared to the GeTe matrix.

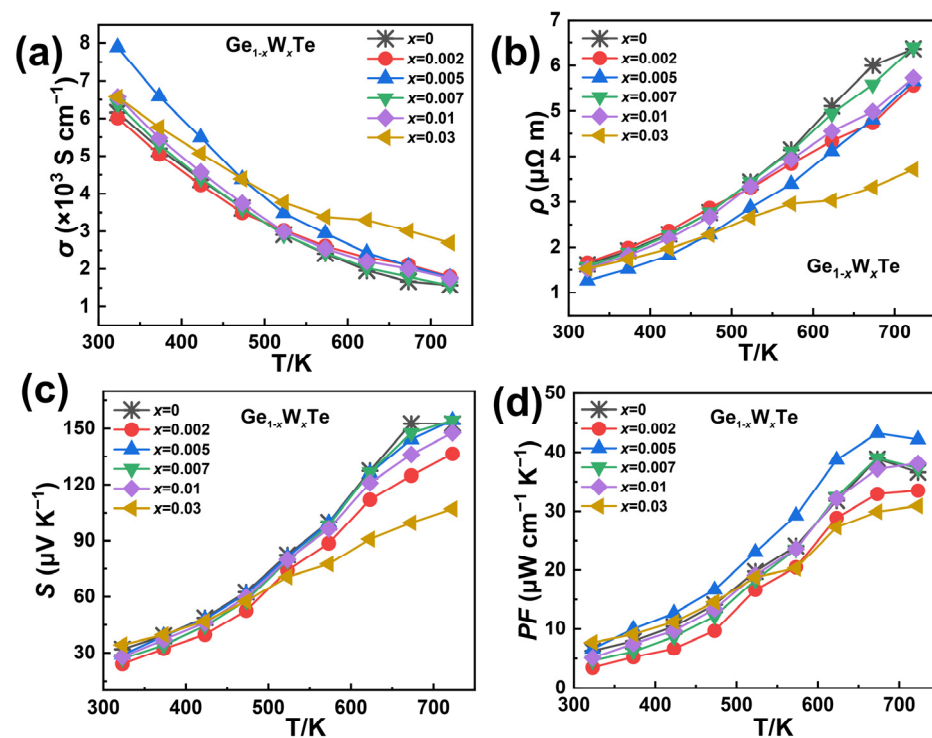


Figure 3. Temperature-dependent electrical performance of the $\text{Ge}_{1-x}\text{W}_x\text{Te}$ ($x = 0, 0.002, 0.005, 0.007, 0.01, 0.03$) solid solution; (a) electrical conductivity σ ; (b) resistivity ρ ; (c) Seebeck coefficient S ; (d) power factor PF.

In Figure 4a, for the $\text{Ge}_{1-x}\text{W}_x\text{Te}$ samples ($x = 0, 0.002, 0.005, 0.007, 0.01, 0.03$), at $x = 0.002$, the total thermal conductivity κ_{tot} exhibits a slight decrease compared to the undoped sample, while at $x = 0.005$, the change in κ_{tot} of the sample $\text{Ge}_{0.995}\text{W}_{0.005}\text{Te}$ is minimal, differing only marginally from the sample at $x = 0.002$. As the doping ratio continues to increase, the overall trend of κ_{tot} continues to decrease. At $x = 0.03$, the κ_{tot} of the sample $\text{Ge}_{0.97}\text{W}_{0.03}\text{Te}$ remains relatively flat, and thermal performance deteriorates. This phenomenon is consistent with the earlier XRD findings, where the degradation is attributed to the different forms of W presence in the GeTe system, which significantly affects the carriers, ultimately influencing the thermal transport properties. Additionally, due to

the higher valence state of W compared to Ge^{2+} , it may introduce additional carriers into the system, further increasing the carrier concentration of the GeTe base material, resulting in a higher electronic thermal conductivity κ_e compared to undoped GeTe, with higher proportions of W leading to higher κ_e and a flattening trend. In Figure 4b, the slope of the κ_e curve for the sample $\text{Ge}_{0.97}\text{W}_{0.03}\text{Te}$ decreases, becoming flatter overall. When the W doping ratio reaches $x = 0.005$, the κ_e of the sample $\text{Ge}_{0.995}\text{W}_{0.005}\text{Te}$ reaches $\sim 5.8 \text{ W m}^{-1} \text{ K}^{-1}$ at temperatures near room temperature to 323 K, 29% higher than other samples with different W doping compositions. In Figure 4c, due to the generally higher electronic thermal conductivity κ_e of the $\text{Ge}_{1-x}\text{W}_x\text{Te}$ samples compared to the undoped GeTe base material, the lattice thermal conductivity κ_{lat} of the samples decreases significantly. For instance, the κ_{lat} of the sample $\text{Ge}_{0.998}\text{W}_{0.002}\text{Te}$ reaches a minimum value of $\sim 0.14 \text{ W m}^{-1} \text{ K}^{-1}$ at 673 K, while the κ_{lat} of the sample $\text{Ge}_{0.995}\text{W}_{0.005}\text{Te}$ decreases to $\sim 0.44 \text{ W m}^{-1} \text{ K}^{-1}$ at 673 K. The effective reduction of κ_{lat} in the material is achieved via appropriate W doping into the GeTe system. In Figure 4d, the extremely low κ_{lat} of the sample $\text{Ge}_{0.998}\text{W}_{0.002}\text{Te}$ reduces by approximately 85%, 81%, 79%, 77%, 74%, and 39% compared to the works of Yang et al. on GeTe: Bi, In [35], Liu et al. on GeTe: Mn, Bi [13], Li et al. on GeTe: Cd, Bi [36], Srinivasan et al. on GeTe: Ag [37], Xu et al. on GeTe: Se, Bi [38], and Shuai et al. on GeTe: Ti, Bi [39], respectively.

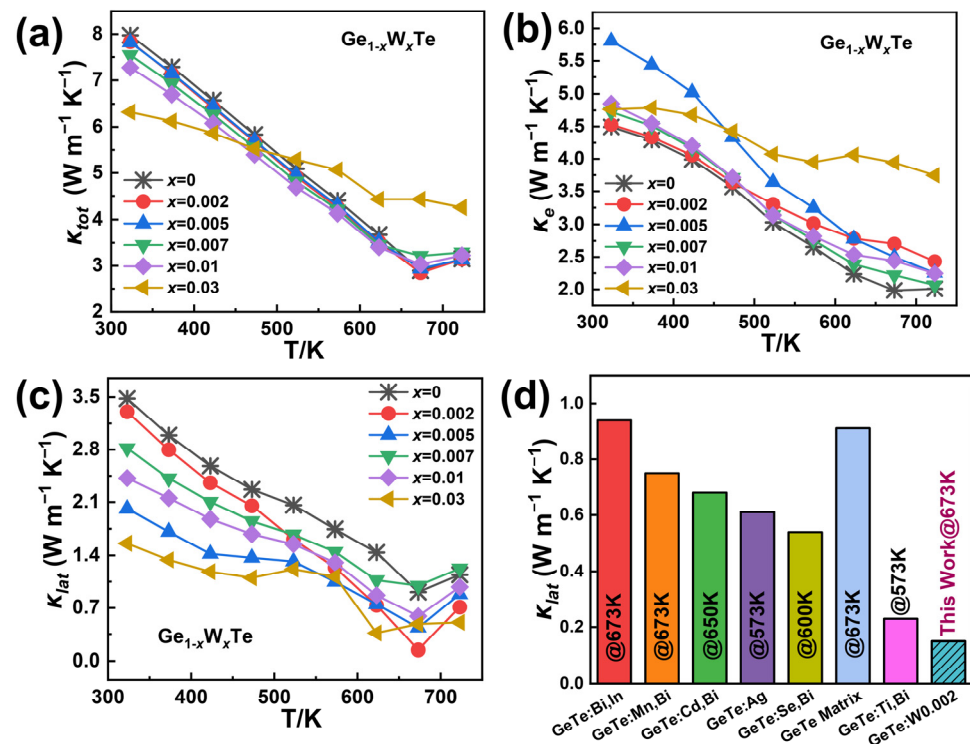


Figure 4. Thermal transport properties of the $\text{Ge}_{1-x}\text{W}_x\text{Te}$ ($x = 0, 0.002, 0.005, 0.007, 0.01, 0.03$) samples; (a) total thermal conductivity κ_{tot} ; (b) electronic thermal conductivity κ_e ; (c) lattice thermal conductivity κ_{lat} ; (d) lattice thermal conductivity of this work compared to the GeTe matrix; GeTe: Bi, In [35]; GeTe: Mn, Bi [13]; GeTe: Cd, Bi [36]; GeTe: Ag [37]; GeTe: Se, Bi [38]; and GeTe: Ti, Bi [39].

In order to further investigate the mechanism of the influence of W doping on the thermoelectric transport properties of the GeTe system and the microstructural morphology of the material, we performed a transmission electron microscopy (TEM) characterization test on the $\text{Ge}_{0.995}\text{W}_{0.005}\text{Te}$ sample. As shown in Figure 5a, a low magnification TEM image of the sample $\text{Ge}_{0.995}\text{W}_{0.005}\text{Te}$ is demonstrated, and the typical herringbone fishbone structure of the GeTe material can be clearly observed [40], which is uniformly interlaced throughout the sample. The magnified image of the orange dashed box area in Figure 5a corresponds to that shown in Figure 5b, and the high-resolution image can better illustrate

the herringbone fishbone structure, from which it can be seen that the W doping of GeTe does not produce a second phase to the microstructure of the material. It also improves the orderliness of the atomic arrangement of the GeTe material. Subsequently, selected area electron diffraction (SAED) was performed on the same sample by choosing the appropriate region. The SAED image of the $\text{Ge}_{0.995}\text{W}_{0.005}\text{Te}$ sample at high magnification along the direction of the $[2\ 1\ 1]$ crystal axis is demonstrated in Figure 5c, from which the diffractograms show that the synthesized sample has a single-crystalline structure and is consistent with the r-GeTe crystalline phase. The angle between the $(\bar{1},1,1)$, $(\bar{2},2,2)$, and $(\bar{1},0,2)$ crystal planes is $\sim 110.7^\circ$, which is slightly smaller than the 120° angle of the GeTe rhombic phase structure, which precisely indicates that the W doping is introduced to more likely substitute the Ge sites and bring about slight nanoscale lattice distortions [41], which agrees with the results of the sample's electrical conductivity test in Figure 3d.

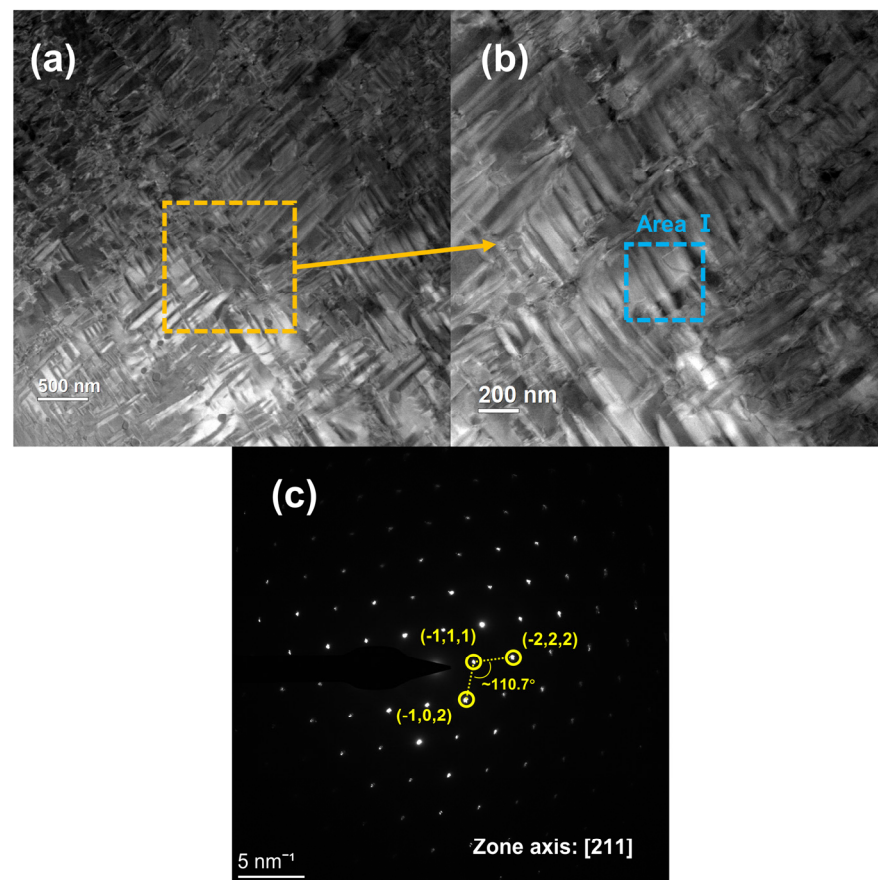


Figure 5. Transmission scanning microscopy (TEM) images of the $\text{Ge}_{0.995}\text{W}_{0.005}\text{Te}$ solid solution: (a) low magnification TEM image; (b) enlarged TEM image of the area surrounded by dashed lines in (a); (c) selected area electron diffraction (SAED) pattern of the GeTe matrix with the $[2\ 1\ 1]$ zone axis.

The blue dashed box area in Figure 5b of the $\text{Ge}_{0.995}\text{W}_{0.005}\text{Te}$ sample was selected to be photographed at high magnification to obtain a high-resolution magnified image, as shown in Figure 6a. It clearly demonstrates that the $\text{Ge}_{0.995}\text{W}_{0.005}\text{Te}$ sample exhibits a pronounced dislocation structure in Figure 6a, resulting from the disparate mass and size of the Ge and W atoms. This leads to the typical lattice distortions observed in W doping at the Ge sites, which introduces defects, optimizes the electron–phonon transport properties of the material, and further enhances the phonon scattering. This is consistent with the findings of our previous work [16], which demonstrated that W is capable of introducing a significant number of defects, thereby greatly reducing the lattice thermal conductivity of the material. In the high-resolution image of Figure 6b, the area within the yellow dashed box represents the interplanar spacing measured for sample $\text{Ge}_{0.995}\text{W}_{0.005}\text{Te}$,

as indicated by the yellow arrows corresponding to Figure 6c,d, which represent the d spacing values of $d_{(202)} \sim 0.3012$ nm and $d_{(202)} \sim 0.3018$ nm, respectively. They are both very close to the standard value of the d spacing of the r -GeTe (202) planar of 2.991 Å. This implies that W doping does not bring about a significant second phase but rather modulates the microstructure of the GeTe material by introducing defects. It is noteworthy that these results are in agreement with the previously mentioned XRD and electrical-thermal performance tests, which significantly enhance the electrical conductivity of the GeTe material.

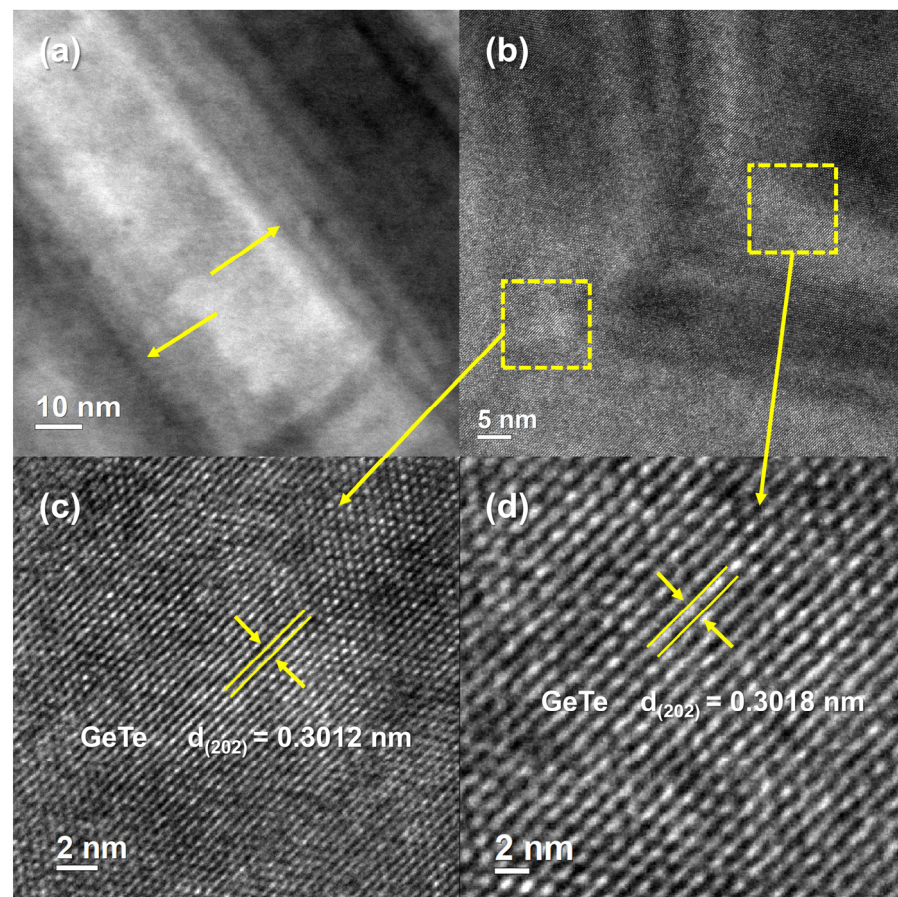


Figure 6. (a) High magnification TEM image of the blue dashed box area (area I) corresponding to Figure 5b of the $\text{Ge}_{0.995}\text{W}_{0.005}\text{Te}$ solid solution; (b) HRTEM image of the same solid solution; (c,d) enlarged HRTEM images corresponding to the area surrounded by yellow dashed lines in (a), respectively.

Figure 7 depicts the temperature-dependent curves of the sample $\text{Ge}_{1-x}\text{W}_x\text{Te}$ ($x = 0, 0.002, 0.005, 0.007, 0.01, 0.03$). When the W doping concentration reaches $x = 0.005$, the ZT value of the sample $\text{Ge}_{0.995}\text{W}_{0.005}\text{Te}$ reaches its maximum, approximately 0.99 at 673 K, 10% higher than the undoped sample. Due to the high melting point of W, in the high-temperature range (573–723 K), the average ZT value of the $\text{Ge}_{1-x}\text{W}_x\text{Te}$ sample is approximately 0.76, 17% higher than the undoped GeTe matrix at the same temperature range. However, a high dopant concentration ($x \geq 0.007$) causes an excess of W in the sample, which leads to a decrease in the carrier mobility due to increased carrier scattering; at the same time, the electronic thermal conductivity κ_e increases (as well as the total thermal conductivity κ_{tot}), leading to a negative optimization in the figure of merit. Therefore, the sample $\text{Ge}_{1-x}\text{W}_x\text{Te}$ achieves the highest ZT value for the $x = 0.005$ doping concentration.

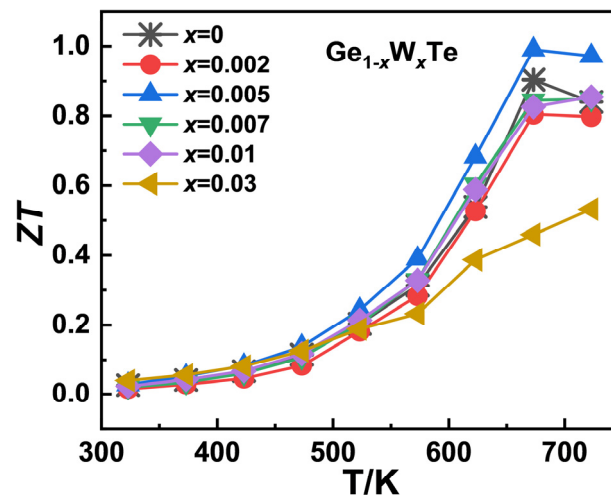


Figure 7. Temperature-dependent trend of the figure of merit (ZT) value of the $\text{Ge}_{1-x}\text{W}_x\text{Te}$ ($x = 0, 0.002, 0.005, 0.007, 0.01, 0.03$) samples.

4. Conclusions

In summary, this study elucidates the advantages and disadvantages of W-doped GeTe materials, analyzing the influence of W on the material structure, electrical transport properties, and thermal transport properties. The higher valence state of W allows for the introduction of additional charge carriers, thereby enhancing the electrical conductivity of the material while simultaneously increasing the power factor, thereby improving the Seebeck coefficient. With a higher melting point than GeTe, W stabilizes the rock-salt cubic structure of GeTe (achieved through the phase transition from r-GeTe) near 700 K. It is noteworthy that W doping can also substitute the Ge atoms in the GeTe material system, introducing dislocation defects to optimize the thermal transport performance. W doping can also induce lattice distortions in the GeTe structure [15], enhancing phonon scattering and effectively reducing the lattice thermal conductivity of the material at suitable W doping concentrations, resulting in GeTe-based materials with ultra-low lattice thermal conductivity as low as approximately $0.14 \text{ W m}^{-1} \text{ K}^{-1}$ at 673 K [16,27,42]. Compared to the previous work [35], this study demonstrates a maximum reduction of approximately 85% in lattice thermal conductivity. The experimental results confirmed that W doping not only introduces high-valence state W atoms to enhance the power factor of the sample but also simultaneously reduces the lattice thermal conductivity by optimizing the material structure [32], thereby comprehensively regulating the thermoelectric transport properties of GeTe-based materials. Ultimately, the average ZT value of the sample $\text{Ge}_{0.995}\text{W}_{0.005}\text{Te}$ reached ~ 0.76 in the temperature range of 573–723 K, approximately 17% higher than undoped GeTe. Furthermore, the peak ZT value of sample $\text{Ge}_{0.995}\text{W}_{0.005}\text{Te}$ reached ~ 0.99 across the entire temperature range, representing a $\sim 10\%$ improvement over the GeTe base material.

Author Contributions: Investigation, methodology, and data curation, Z.C. and K.Z.; Visualization and investigation, C.M., Y.M. and Y.F.; Writing—original draft preparation, Z.C.; Writing—review and editing, Z.C., Q.D. and H.L.; Conceptualization, H.L.; Supervision, H.L.; Funding acquisition, H.L. All authors have read and agreed to the published version of the manuscript.

Funding: This work is funded by the Young Talent Program of Guangzhou University (Grant No. RQ2020077), the Key Discipline of Materials Science and Engineering and Bureau of Education of Guangzhou Municipality (Grant No. 202201020144), Bureau of Education of Guangzhou Municipality (Grant No. 202255464) and the China Biosafety Research Special Program (Grant No. 20SWAQX40).

Data Availability Statement: Data are contained within the article.

Conflicts of Interest: The authors declare no conflicts of interest.

References

1. Mao, J.; Liu, Z.H.; Zhou, J.W.; Zhu, H.T.; Zhang, Q.; Chen, G.; Ren, Z.F. Advances in thermoelectrics. *Adv. Phys.* **2018**, *67*, 69–147. [[CrossRef](#)]
2. Yang, L.; Chen, Z.G.; Dargusch, M.S.; Zou, J. High Performance Thermoelectric Materials: Progress and Their Applications. *Adv. Energy Mater.* **2017**, *8*, 1701797–1701824. [[CrossRef](#)]
3. Zhang, X.; Bu, Z.; Lin, S.; Chen, Z.; Li, W.; Pei, Y. GeTe Thermoelectrics. *Joule* **2020**, *4*, 986–1003. [[CrossRef](#)]
4. Liu, Z.H.; Gao, W.H.; Zhang, W.H.; Sato, N.; Guo, Q.S.; Mori, T. High Power Factor and Enhanced Thermoelectric Performance in Sc and Bi Codoped GeTe: Insights into the Hidden Role of Rhombohedral Distortion Degree. *Adv. Energy Mater.* **2020**, *10*, 202002588–202002597. [[CrossRef](#)]
5. Hong, M.; Lyv, W.Y.; Li, M.; Xu, S.D.; Sun, Q.; Zou, J.; Chen, Z.G. Rashba Effect Maximizes Thermoelectric Performance of GeTe Derivatives. *Joule* **2020**, *4*, 2030–2043. [[CrossRef](#)]
6. Srinivasan, B.; Le Tonquesse, S.; Gellé, A.; Bourgès, C.; Monier, L.; Ohkubo, I.; Halet, J.F.; Berthebaud, D.; Mori, T. Screening of transition (Y, Zr, Hf, V, Nb, Mo, and Ru) and rare-earth (La and Pr) elements as potential effective dopants for thermoelectric GeTe—An experimental and theoretical appraisal. *J. Mater. Chem. A* **2020**, *8*, 19805–19821. [[CrossRef](#)]
7. Kihoi, S.K.; Shenoy, U.S.; Kahi, J.N.; Kim, H.; Bhat, D.K.; Lee, H.S. Ultralow Lattice Thermal Conductivity and Enhanced Mechanical Properties of Cu and Sb Co-Doped SnTe Thermoelectric Material with a Complex Microstructure Evolution. *ACS Sustain. Chem. Eng.* **2022**, *10*, 1367–1372. [[CrossRef](#)]
8. Huo, H.; Wang, Y.; Xi, L.; Yang, J.; Zhang, W. The variation of intrinsic defects in XTe (X = Ge, Sn, and Pb) induced by the energy positions of valence band maxima. *J. Mater. Chem. C* **2021**, *9*, 5765–5770. [[CrossRef](#)]
9. Lei, K.; Huang, H.M.; Liu, X.J.; Wang, W.L.; Guo, K.; Zheng, R.K.; Li, H. Ultra-Low Lattice Thermal Conductivity Enables High Thermoelectric Properties in Cu and Y Codoped SnTe via Multi-Scale Composite Nanostructures. *ACS Sustain. Chem. Eng.* **2023**, *11*, 7541–7551. [[CrossRef](#)]
10. Ge, B.Z.; Lee, H.; Im, J.; Choi, Y.; Kim, S.Y.; Lee, J.Y.; Cho, S.P.; Sung, Y.E.; Choi, K.Y.; Zhou, C.J.; et al. Engineering an atomic-level crystal lattice and electronic band structure for an extraordinarily high average thermoelectric figure of merit in n-type PbSe. *Energy Environ. Sci.* **2023**, *16*, 3994–4008. [[CrossRef](#)]
11. Biswas, K.; He, J.; Zhang, Q.; Wang, G.; Uher, C.; Dravid, V.P.; Kanatzidis, M.G. Strained endotaxial nanostructures with high thermoelectric figure of merit. *Nat. Chem.* **2011**, *3*, 160–166. [[CrossRef](#)] [[PubMed](#)]
12. Pei, Y.; Shi, X.; LaLonde, A.; Wang, H.; Chen, L.; Snyder, G.J. Convergence of electronic bands for high performance bulk thermoelectrics. *Nature* **2011**, *473*, 66–69. [[CrossRef](#)] [[PubMed](#)]
13. Liu, Z.; Sun, J.; Mao, J.; Zhu, H.; Ren, W.; Zhou, J.; Wang, Z.; Singh, D.J.; Sui, J.; Chu, C.W.; et al. Phase-transition temperature suppression to achieve cubic GeTe and high thermoelectric performance by Bi and Mn codoping. *Proc. Natl. Acad. Sci. USA* **2018**, *115*, 5332–5337. [[CrossRef](#)] [[PubMed](#)]
14. Cahill, D.G.; Watson, S.K.; Pohl, R.O. Lower limit to the thermal conductivity of disordered crystals. *Phys. Rev. B Condens. Matter* **1992**, *46*, 6131–6140. [[CrossRef](#)] [[PubMed](#)]
15. Li, J.; Zhang, X.; Chen, Z.; Lin, S.; Li, W.; Shen, J.; Witting, I.T.; Faghaninia, A.; Chen, Y.; Jain, A.; et al. Low-Symmetry Rhombohedral GeTe Thermoelectrics. *Joule* **2018**, *2*, 976–987. [[CrossRef](#)]
16. Lei, K.; Feng, K.m.; Ma, C.; Cai, Z.T.; He, B.b.; Li, H. High power factor and ultra-low lattice thermal conductivity in $\text{Sn}_{1-x}\text{W}_x\text{Te}$ alloys via interstitial defects modulation. *J. Alloys Compd.* **2024**, *976*, 173187. [[CrossRef](#)]
17. Wang, G.; Zhou, J.; Sun, Z. First principles investigation on anomalous lattice shrinkage of W alloyed rock salt GeTe. *J. Phys. Chem. Solids* **2020**, *137*, 109220. [[CrossRef](#)]
18. Zheng, L.; Li, W.; Lin, S.; Li, J.; Chen, Z.; Pei, Y. Interstitial Defects Improving Thermoelectric SnTe in Addition to Band Convergence. *ACS Energy Lett.* **2017**, *2*, 563–568. [[CrossRef](#)]
19. Yin, L.C.; Liu, W.D.; Li, M.; Wang, D.Z.; Wu, H.; Wang, Y.F.; Zhang, L.X.; Shi, X.L.; Liu, Q.F.; Chen, Z.G. Interstitial Cu: An Effective Strategy for High Carrier Mobility and High Thermoelectric Performance in GeTe. *Adv. Funct. Mater.* **2023**, *33*, 2301750–2301758. [[CrossRef](#)]
20. Xin, J.; Li, S.; Yang, J.; Basit, A.; Long, Q.; Li, S.; Jiang, Q.; Xu, T.; Xiao, B. Tactfully decoupling interdependent electrical parameters via interstitial defects for SnTe thermoelectrics. *Nano Energy* **2020**, *67*, 104292. [[CrossRef](#)]
21. Foster, A.S.; Lopez Gejo, F.; Shluger, A.L.; Nieminen, R.M. Vacancy and interstitial defects in hafnia. *Phys. Rev. B* **2002**, *65*, 174117. [[CrossRef](#)]
22. Li, H.; Jing, H.; Han, Y.; Lu, G.-Q.; Xu, L.; Liu, T. Interfacial evolution behavior of AgSbTe_{2.01}/nanosilver/Cu thermoelectric joints. *Mater. Des.* **2016**, *89*, 604–610. [[CrossRef](#)]
23. Li, J.; Zhang, X.; Lin, S.; Chen, Z.; Pei, Y. Realizing the High Thermoelectric Performance of GeTe by Sb-Doping and Se-Alloying. *Chem. Mater.* **2016**, *29*, 605–611. [[CrossRef](#)]
24. Liu, H.; Zhang, X.; Li, J.; Bu, Z.; Meng, X.; Ang, R.; Li, W. Band and Phonon Engineering for Thermoelectric Enhancements of Rhombohedral GeTe. *ACS Appl. Mater. Interfaces* **2019**, *11*, 30756–30762. [[CrossRef](#)] [[PubMed](#)]
25. Su, L.; Wang, D.; Wang, S.; Qin, B.; Wang, Y.; Qin, Y.; Jin, Y.; Chang, C.; Zhao, L.D. High thermoelectric performance realized through manipulating layered phonon-electron decoupling. *Science* **2022**, *375*, 1385–1389. [[CrossRef](#)] [[PubMed](#)]

26. Li, M.R.; Ying, P.Z.; Du, Z.L.; Liu, X.L.; Li, X.; Fang, T.; Cui, J.L. Improved Thermoelectric Performance of P-type SnTe through Synergistic Engineering of Electronic and Phonon Transports. *ACS Appl. Mater. Interfaces* **2022**, *14*, 8171–8178. [[CrossRef](#)] [[PubMed](#)]
27. Xing, T.; Zhu, C.; Song, Q.; Huang, H.; Xiao, J.; Ren, D.; Shi, M.; Qiu, P.; Shi, X.; Xu, F.; et al. Ultralow Lattice Thermal Conductivity and Superhigh Thermoelectric Figure-of-Merit in (Mg, Bi) Co-Doped GeTe. *Adv. Mater.* **2021**, *33*, e2008773. [[CrossRef](#)] [[PubMed](#)]
28. Wu, Z.; Chen, X.; Mu, E.; Liu, Y.; Che, Z.; Dun, C.; Sun, F.; Wang, X.; Zhang, Y.; Hu, Z. Lattice Strain Enhances Thermoelectric Properties in Sb₂Te₃/Te Heterostructure. *Adv. Electron. Mater.* **2019**, *6*, 1900735. [[CrossRef](#)]
29. Wu, G.J.; Guo, Z.; Wang, R.Y.; Tan, X.J.; Cui, C.; Sun, P.; Hu, H.Y.; Wu, J.H.; Liu, G.Q.; Jiang, J. Structural modulation and resonant level enable high thermoelectric performance of GeTe in the mid-to-low temperature range. *J. Mater. Chem. A* **2023**, *11*, 20497–20505. [[CrossRef](#)]
30. Jin, Y.; Wang, D.Y.; Qiu, Y.T.; Zhao, L.D. Boosting the thermoelectric performance of GeTe by manipulating the phase transition temperature Sb doping. *J. Mater. Chem. C* **2021**, *9*, 6484–6490. [[CrossRef](#)]
31. Pei, Q.-X.; Guo, J.-Y.; Suwardi, A.; Zhang, G. Insights into interfacial thermal conductance in Bi₂Te₃-based systems for thermoelectrics. *Mater. Today Phys.* **2023**, *30*, 100953. [[CrossRef](#)]
32. Perumal, S.; Samanta, M.; Ghosh, T.; Shenoy, U.S.; Bohra, A.K.; Bhattacharya, S.; Singh, A.; Waghmare, U.V.; Biswas, K. Realization of High Thermoelectric Figure of Merit in GeTe by Complementary Co-doping of Bi and In. *Joule* **2019**, *3*, 2565–2580. [[CrossRef](#)]
33. Hong, M.; Zou, J.; Chen, Z.G. Thermoelectric GeTe with Diverse Degrees of Freedom Having Secured Superhigh Performance. *Adv. Mater.* **2019**, *31*, e1807071. [[CrossRef](#)] [[PubMed](#)]
34. Gao, W.H.; Liu, Z.H.; Zhang, W.H.; Sato, N.; Guo, Q.S.; Mori, T. Improved thermoelectric performance of GeTe via efficient yttrium doping. *Appl. Phys. Lett.* **2021**, *118*, 033901. [[CrossRef](#)]
35. Jin, Y.; Wang, D.; Zhu, Y.; Su, L.; Hong, T.; Wang, Z.; Ge, Z.-H.; Qiu, Y.; Zhao, L.-D. Contrasting roles of trivalent dopants M (M = In, Sb, Bi) in enhancing the thermoelectric performance of Ge_{0.94}M_{0.06}Te. *Acta Mater.* **2023**, *252*, 118926. [[CrossRef](#)]
36. Li, J.; Li, W.; Bu, Z.; Wang, X.; Gao, B.; Xiong, F.; Chen, Y.; Pei, Y. Thermoelectric Transport Properties of Cd_xBi_yGe_{1-x-y}Te Alloys. *ACS Appl. Mater. Interfaces* **2018**, *10*, 39904–39911. [[CrossRef](#)] [[PubMed](#)]
37. Srinivasan, B.; Gautier, R.; Gucci, F.; Fontaine, B.; Halet, J.-F.; Chevire, F.; Boussard-Pledel, C.; Reece, M.J.; Bureau, B. Impact of Coinage Metal Insertion on the Thermoelectric Properties of GeTe Solid-State Solutions. *J. Phys. Chem. C* **2017**, *122*, 227–235. [[CrossRef](#)]
38. Xu, L.; Wu, G.; Wang, R.; Yan, Z.; Cai, J.; Yang, J.; Wang, X.; Luo, J.; Tan, X.; Liu, G.; et al. Synergistically Optimized Thermal Conductivity and Carrier Concentration in GeTe by Bi-Se Codoping. *ACS Appl. Mater. Interfaces* **2022**, *14*, 14359–14366. [[CrossRef](#)] [[PubMed](#)]
39. Shuai, J.; Tan, X.J.; Guo, Q.; Xu, J.T.; Gellé, A.; Gautier, R.; Halet, J.F.; Failamani, F.; Jiang, J.; Mori, T. Enhanced thermoelectric performance through crystal field engineering in transition metal-doped GeTe. *Mater. Today Phys.* **2019**, *9*, 100094. [[CrossRef](#)]
40. Rinaldi, C.; Rojas-Sánchez, J.C.; Wang, R.N.; Fu, Y.; Oyarzun, S.; Vila, L.; Bertoli, S.; Asa, M.; Baldrati, L.; Cantoni, M.; et al. Evidence for spin to charge conversion in GeTe(111). *APL Mater.* **2016**, *4*, 032501. [[CrossRef](#)]
41. Zheng, Z.; Su, X.; Deng, R.; Stoumpos, C.; Xie, H.; Liu, W.; Yan, Y.; Hao, S.; Uher, C.; Wolverton, C.; et al. Rhombohedral to Cubic Conversion of GeTe via MnTe Alloying Leads to Ultralow Thermal Conductivity, Electronic Band Convergence, and High Thermoelectric Performance. *J. Am. Chem. Soc.* **2018**, *140*, 2673–2686. [[CrossRef](#)] [[PubMed](#)]
42. Banik, A.; Vishal, B.; Perumal, S.; Datta, R.; Biswas, K. The origin of low thermal conductivity in Sn_{1-x}Sb_xTe: Phonon scattering via layered intergrowth nanostructures. *Energy Environ. Sci.* **2016**, *9*, 2011–2019. [[CrossRef](#)]

Disclaimer/Publisher's Note: The statements, opinions and data contained in all publications are solely those of the individual author(s) and contributor(s) and not of MDPI and/or the editor(s). MDPI and/or the editor(s) disclaim responsibility for any injury to people or property resulting from any ideas, methods, instructions or products referred to in the content.